

ENERGY EVOLUTION EQUATION FOR ELASTIC SCATTERING AMPLITUDES OF HADRONS IN b -SPACE*

HIREN KAKKAD, ANDERSON KENDI KOHARA, PIOTR KOTKO

AGH University of Science and Technology
Faculty of Physics and Applied Computer Science
Mickiewicza 30, 30-059 Kraków, Poland

*Received 30 November 2022, accepted 30 January 2023,
published online 25 May 2023*

Basing our study on the Regge field theory, we formulate and solve numerically an energy evolution equation for the complex elastic scattering amplitude. The equation is a complex version of the Fisher–Kolmogorov–Petrovsky–Piscounov equation in the impact parameter space. We compare the resulting amplitudes with the experimental data, numerically demonstrate the existence of the fixed points, and discuss the recently discovered scaling.

DOI:10.5506/APhysPolBSupp.16.5-A3

1. Introduction

Due to its kinematic simplicity, elastic scattering of hadrons is one of the most important processes in particle physics, probing electromagnetic interactions at very small scattering angles, non-perturbative strong interactions from small to moderate angles, and perturbative Quantum Chromodynamics (QCD) at very large angles. Measurements of the cross sections as a function of transferred momentum squared $t = -\mathbf{q}^2$ (related directly to the scattering angle) exhibit a characteristic diffractive pattern: the cross section falls rather rapidly, then reaches a dip (a local minimum), next a bump (a local maximum), and finally decays rather slowly for large $|t|$. In the present work, we are interested in a broad t range where the non-perturbative QCD dominates, from the origin ($|t| = 0$) to the region around the dip-bump structure.

Basing our study on the Regge field theory (RFT) [1–4], we have presented in Ref. [5] an energy evolution equation for the complex elastic scattering amplitude in the impact parameter space $b = |\mathbf{b}|$ (conjugate to the

* Presented by A.K. Kohara at the Diffraction and Low- x 2022 Workshop, Corigliano Calabro, Italy, 24–30 September, 2022.

momentum transfer \mathbf{q}). We have also performed a detailed numeric study of the solutions and comparison to data. The work has been done independently of [6], which we were not aware of, where a similar equation was considered, however, with different goals and in isolation from the experimental data.

The purpose of the following paper is not only to report our previous results [5], but also to extend the original study to include the recently discussed scaling properties of the elastic amplitude [7].

2. Evolution equation for elastic amplitude

The starting point is the RFT Lagrangian density proposed in the 1970s [2],

$$\mathcal{L} = \frac{1}{2}q \overleftrightarrow{\partial}_\tau p + \alpha' \nabla_b q \cdot \nabla_b p - \epsilon_0 q p + \lambda q (p + q) p, \quad (1)$$

where the fields q and p are related to Gribov's Pomeron fields, $q = i\bar{\Psi}$, $p = i\Psi$ depending both on b and τ , α' is the Pomeron slope, ϵ_0 is the Pomeron intercept, and λ is the triple Pomeron coupling. The Lagrangian density (1) gives rise to the Hamiltonian \mathcal{H} with the Schrödinger equation

$$\frac{\partial}{\partial \tau} |\psi\rangle = -\mathcal{H} |\psi\rangle, \quad (2)$$

where $|\psi\rangle$ is a generalized coherent state written in terms of higher-order Pomeron correlation functions. In the semi-classical approximation, the Schrödinger equation reduces to the Hamilton–Jacobi equation which is a partial differential equation for the two-point correlation function. In our work, we assume that the energy behaviour of the two-point correlation function determines behaviour of the complex elastic scattering amplitudes and consequently its S-matrix elements, leading to the following differential equation:

$$\frac{\partial \tilde{\mathcal{S}}(\tau, \mathbf{b})}{\partial \tau} = \alpha' \nabla_{\mathbf{b}}^2 \tilde{\mathcal{S}}(\tau, \mathbf{b}) - \epsilon_0 \left(1 - \tilde{\mathcal{S}}(\tau, \mathbf{b})\right) + \lambda \left(1 - \tilde{\mathcal{S}}(\tau, \mathbf{b})\right)^2, \quad (3)$$

where $1 - \tilde{\mathcal{S}} = \tilde{T}_I - i\tilde{T}_R$. In the large impact parameter approximation, separating the real and imaginary parts of the amplitudes, we obtain two coupled partial differential equations

$$\frac{\partial \tilde{T}_I}{\partial \tau} = \alpha' \frac{\partial^2 \tilde{T}_I}{\partial b^2} + \epsilon_0 \left[\tilde{T}_I \left(1 - \frac{\lambda}{\epsilon_0} \tilde{T}_I\right) + \frac{\lambda}{\epsilon_0} \tilde{T}_R^2 \right], \quad (4)$$

and

$$\frac{\partial \tilde{T}_R}{\partial \tau} = \alpha' \frac{\partial^2 \tilde{T}_R}{\partial b^2} + \epsilon_0 \tilde{T}_R \left(1 - 2 \frac{\lambda}{\epsilon_0} \tilde{T}_I\right). \quad (5)$$

3. Numerical results

The numerical solution for the coupled set of differential equations (4)–(5) was presented and discussed in detail in [5]. Here, we highlight the strategy and the main results.

In order to solve the differential equations (4)–(5) numerically, we use the Kohara–Ferreira–Kodama (KFK) model [8, 9] and independently the Bourrely–Soffer–Wu (BSW) model [10] based on b -space profiles for \tilde{T}_1 and \tilde{T}_R as initial conditions at $\sqrt{s} = 500$ GeV. The values of the three parameters (λ , ϵ_0 , α') are determined by fitting the differential cross section at a given energy and the cross sections for the remaining energies come as predictions. In our case, we fit TOTEM data at 13 TeV (it has better statistics and small fluctuations). The values are shown in Table 1.

Table 1. The parameters α' , ϵ_0 , and λ for different initial conditions.

	α' [GeV ⁻²]	ϵ_0	λ/ϵ_0
KFK	0.105	0.129	0.712
BSW	0.010	0.150	0.770

It is interesting to observe that the obtained Pomeron intercept ϵ_0 is relatively larger than the standard critical value $\epsilon_0 = 0.096$, and the average value of the triple Pomeron coupling λ extracted from Table 1 is 0.103 (close to 0.096). This should not appear as a surprise because unitarity in b -space constrains $\lambda = \epsilon_0$ [6]. However, what is interesting is that the Pomeron slope is rather small compared to the standard value of 0.25 GeV⁻². This possibility was already predicted in the 1970s.

In Fig. 1, we compare the results of our equation with the available TOTEM data. In the left figure, up to the dip, including its position (see Table 2) and magnitude, there is good agreement between TOTEM measurements and our predictions represented via bands, which are obtained using the results for the two initial conditions, KFK and BSW. In the right panel of Fig. 1, the very forward part is in excellent agreement with TOTEM measurements for 2.76, 7, 8, and 13 TeV. However, beyond the bump our curves go below the TOTEM measurements. We suspect this is due to the lack of other interaction vertices in the Lagrangian.

According to recent discussions about the Odderon, potentially observed in LHC energies, the comparison between pp and $p\bar{p}$ processes is crucial. However, at high energies, there are no experiments performed at the same energy for these two processes. The comparison between them at different energies is possible by some change of variables [7], stacking up the differential cross sections measured in different energies. Since our amplitude

reproduces the LHC data, we write our solutions in terms of this change of variables and we observe approximate scaling, except for the very forward part and beyond the dip.

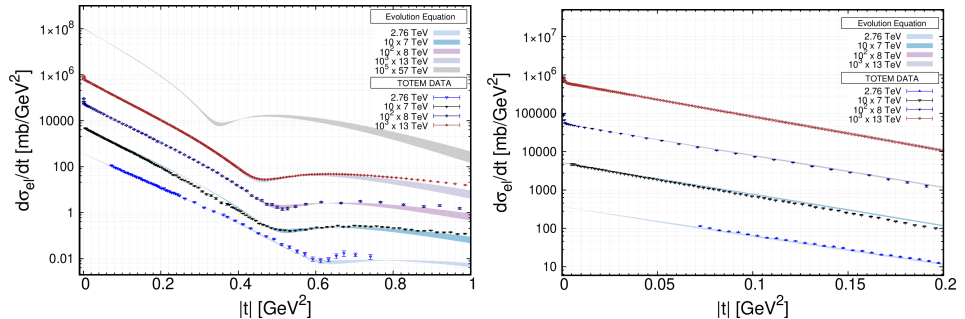


Fig. 1. Left: The points represent the TOTEM p - p elastic differential cross section, whereas the bands represent the prediction from our equation for the KFK and BSW initial conditions. Right: The very forward part, up to $|t| = 0.2 \text{ GeV}^2$, of the elastic differential cross section.

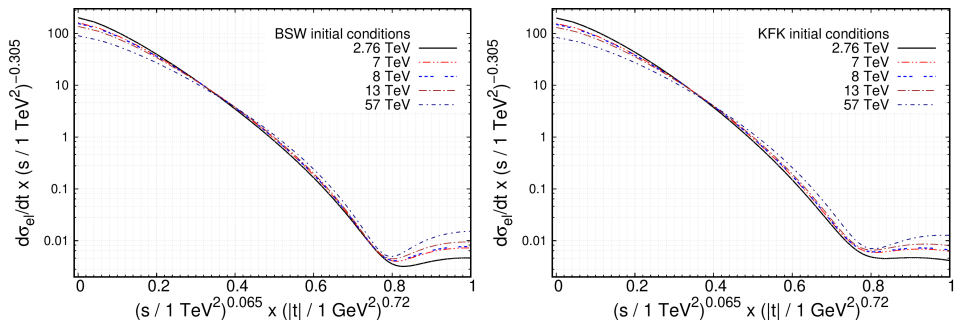


Fig. 2. We show our results re-scaled according to Ref. [7] from the LHC energies up to Cosmic Ray at 57 TeV. It is interesting to note that despite the fixed position of the dip, the shape of the differential cross section deviates for larger energies.

In Fig. 3, we present the amplitudes in t -space. Notice that the first zero of the real amplitudes precedes that of the imaginary amplitudes as shown on the left in Fig. 3; and, as the energy increases, the former approaches the origin prior to the latter as expected from Martin's theorem [11]. The location of the latter is crucial for determining the t -dip. Another interesting aspect is the presence of two fixed points for each \tilde{T}_I and \tilde{T}_R profile [12]. These fixed points occur on the either side of the first zero for both amplitudes. The first fixed point, shown on the right in Fig. 3, appears in the very forward range: $|t| = 0.07 \text{ GeV}^2$ and 0.2 GeV^2 for \tilde{T}_R and \tilde{T}_I , respectively, whereas the second fixed point appears at $|t| = 0.5 \text{ GeV}^2$ and 1 GeV^2 as shown on the left in Fig. 3.

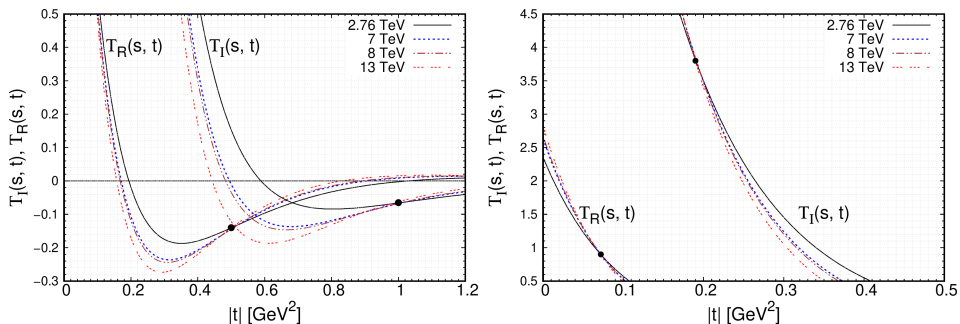


Fig. 3. Left: Real and imaginary amplitudes obtained from our equation for the KFK initial condition for different energies seem to contain a fixed point beyond the first zero. Right: The second fixed point in the amplitudes is in the very forward part.

In Table 2, we show the derived quantities computed using our evolution equation for both the initial conditions. The computed total cross section σ_{tot} for different energies is in good agreement with the TOTEM [13] and

Table 2. We show the derived quantities obtained from our equation with the two initial conditions (KFK and BSW), the corresponding LHC experimental data (TOTEM [13]/ATLAS [14]), and the Cosmic Ray data (AUGER [15]).

	\sqrt{s} [TeV]	σ_{tot} [mb]	ρ	B [GeV^{-2}]	t_{dip} [GeV^2]
KFK initial condition	2.76	84.31	0.123	17.28	0.65
	7	99.07	0.117	18.47	0.53
	8	101.32	0.116	18.65	0.51
	13	109.78	0.113	19.32	0.46
	57	138.32	0.105	21.55	0.36
BSW initial condition	2.76	84.94	0.113	19.23	0.64
	7	100.97	0.105	20.41	0.53
	8	103.41	0.104	20.59	0.51
	13	112.62	0.101	21.27	0.46
	57	143.66	0.091	23.59	0.35
TOTEM	2.76	84.7 ± 3.3	—	17.1 ± 0.30	0.61 ± 0.03
	7	98.0 ± 2.5	0.145 ± 0.091	19.73 ± 0.40	0.53 ± 0.01
	8	101.7 ± 2.9	0.12 ± 0.03	19.74 ± 0.28	0.52 ± 0.01
	13	110.6 ± 3.4	0.10 ± 0.01	20.40 ± 0.01	0.47 ± 0.004
ATLAS	7	95.35 ± 0.38	0.14 (fix)	19.73 ± 0.14	—
	8	96.07 ± 0.18	0.136 (fix)	19.74 ± 0.05	—
AUGER	57	133 ± 29	—	—	—

AUGER [15] measurements. The ρ predictions for 7, 8, and 13 TeV are well within the error limits of TOTEM measurements. For B , the average of real and imaginary slopes, the measured values fall in between our predictions for the two initial conditions.

4. Summary

In the present work, we discuss the evolution equation for elastic scattering amplitudes based on the Regge Field Theory, transforming elastic scattering of hadrons into an initial value problem. Using phenomenological models for the real and imaginary profiles as initial conditions, we reproduce the differential cross sections measured in the LHC energies in a broad t range, from $|t| = 0$ to the dip-bump region. With only three physical parameters, the equation can accurately reproduce not only the differential cross section but also the derived quantities such as σ_{tot} , ρ , the average differential cross section slope B , and the elastic integrated cross section σ_{el} . We can safely extrapolate and interpolate our results: we show some interesting features such as the existence of fixed points in the amplitudes in t -space for a broad s range and we reproduce the scaling in the LHC range, recently discussed in interpretation of the Odderon.

H.K. is supported by the National Science Centre, Poland (NCN) grant No. 2021/41/N/ST2/02956, A.K.K. is supported by the National Science Centre, Poland (NCN) grant No. 2020/37/K/ST2/02665, and P.K. is supported by the National Science Centre, Poland (NCN) grant No. 2020/39/O/ST2/03011. The research leading to these results has received funding from the Norwegian Financial Mechanism 2014–2021.

REFERENCES

- [1] V.N. Gribov, *Zh. Eksp. Teor. Fiz.* **53**, 654 (1967).
- [2] H.D.I. Abarbanel, J.D. Bronzan, R.L. Sugar, A.R. White, *Phys. Rep.* **21**, 119 (1975).
- [3] D. Amati, L. Bellac, G. Marchesini, M. Ciafaloni, *Nucl. Phys. B* **112**, 101 (1976).
- [4] V. Alessandrini, D. Amati, R. Jengo, *Nucl. Phys. B* **108**, 425 (1976).
- [5] H. Kakkad, A.K. Kohara, P. Kotko, *Eur. Phys. J. C* **82**, 830 (2022).
- [6] R. Peschanski, *Phys. Rev. D* **79**, 105014 (2009).
- [7] C. Baldenegro, C. Royon, A.M. Stasto, *Phys. Lett. B* **830**, 137141 (2022).
- [8] A.K. Kohara, E. Ferreira, T. Kodama, *Eur. Phys. J. C* **74**, 3175 (2014).
- [9] E. Ferreira, A.K. Kohara, T. Kodama, *Eur. Phys. J. C* **81**, 4 (2021).
- [10] C. Bourrely, J. Soffer, T.T. Wu, *Phys. Rev. D* **19**, 3249 (1979).
- [11] A. Martin, *Phys. Lett. B* **404**, 137 (1997).

- [12] T. Csörgő, I. Szanyi, International Scientific Days — Femtoscopy Session, 2022, <https://indico.cern.ch/event/1152630/>
- [13] TOTEM Collaboration (G. Antchev *et al.*), *Eur. Phys. J. C* **80**, 91 (2020); *Europhys. Lett.* **101**, 21002 (2013); *Eur. Phys. J. C* **76**, 661 (2016); *ibid.* **79**, 103 (2019).
- [14] ATLAS Collaboration (G. Aad *et al.*), *Nucl. Phys. B* **889**, 486 (2014); *Phys. Lett. B* **761**, 158 (2016).
- [15] The Pierre Auger Collaboration (P. Abreu *et al.*), *Phys. Rev. Lett.* **109**, 062002 (2012).